Scaling laws and accurate small-amplitude stationary solution for the motion of a planar vortex filament in the Cartesian form of the local induction approximation

Robert A. Van Gorder

Phys. Rev. E **87**, 043203 — Published 23 April 2013

DOI: 10.1103/PhysRevE.87.043203

Scaling laws and accurate small-amplitude stationary solution for the motion of a planar vortex filament in the Cartesian form of the local induction approximation

Robert A. Van Gorder
Department of Mathematics, University of Central Florida, Orlando, FL 32816-1364 USA
rav@knights.ucf.edu

We provide a formulation of the local induction approximation (LIA) for the motion of a vortex filament in the Cartesian reference frame (the extrinsic coordinate system) which allows for scaling of the reference coordinate. For general monotone scalings of the reference coordinate, we derive an equation for the planar solution to the derivative nonlinear Schrödinger equation governing the LIA. We proceed to solve this equation perturbatively in small amplitude through an application of multiple scales analysis, which allows for accurate computation of the period of the planar vortex filament. The perturbation result is shown to agree strongly with numerical simulations, and we also relate this solution back to the solution obtained in the arclength reference frame (the intrinsic coordinate system). Finally, we discuss non-monotone coordinate scalings and their application for finding self-intersections of vortex filaments. These self-intersecting vortex filaments are likely unstable and collapse into other structures or dissipate completely.
Keywords: Vortex dynamics; Vortex filament; Local induction approximation; planar vortex filament

PACS numbers: 47.32.C-

I. INTRODUCTION

The self-induced velocity of a vortex filament has been described by the local induction approximation (LIA) $\mathbf{v} = \gamma\kappa\mathbf{t}\times\mathbf{n}$ (Da Rios [1], Arms and Hama [2], Ricca [3]), where $\mathbf{t}$ and $\mathbf{n}$ are unit tangent and unit normal vectors to the vortex filament, respectively, κ is the curvature and γ is the strength of the vortex filament. A number of methods have been employed to study the LIA. Exact stationary solutions to the LIA in extrinsic coordinate space have been found by Kida [4] in the case of torus knots, and these solutions were given in terms of elliptic integrals. By re-writing the LIA in cylindrical-polar coordinates, Ricca also obtained torus knot solutions - which were asymptotically equivalent to Kida's solutions - in explicit analytic form and derived a stability criterion [5]. Static solutions to the LIA have also been found by Lipniacki [6]. Physical invariants obtained under LIA were discussed in Ricca [7].

The fully nonlinear Schrödinger (NLS) equation governing the self-induced motion of a vortex filament in the LIA was previously derived in Van Gorder [8, 9] in the Cartesian coordinate space. Dmitriyev [10] considered a linear approximation to the LIA, while Shivamoggi and van Heijst [11] considered a more sophisticated approximation, obtaining a cubic derivative NLS equation. The full nonlinear equation was obtained in [8]. Some existence results for space-periodic planar vortex filaments are given in a forthcoming work. In particular, it was shown that there exists a maximal amplitude beyond which space-periodic planar vortex filament solutions do not exist. We should remark that the aforementioned studies considered the Cartesian form of the LIA. Umeki [12] obtained an alternate formulation, applying an arclength-based coordinate system as opposed to a Cartesian coordinate system. While the Cartesian and arc-length formulations are obtained through different derivations, both formulations are equivalent to the LIA. Van Gorder [13] obtained exact stationary solutions for this model in terms of elliptic functions.

In the present paper, we provide a formulation of the local induction approximation (LIA) for the motion of a vortex filament in the Cartesian reference frame (the extrinsic coordinate system) which allows for scaling of the reference coordinate. For general monotone scalings of the reference coordinate, we derive an equation for the planar solution to the derivative nonlinear Schrödinger equation governing the LIA. We proceed to solve this equation perturbatively in small amplitude through an application of multiple scales analysis, which allows for accurate computation of the period of the planar vortex filament. The perturbation result is shown to agree strongly with numerical simulations, and we also relate this solution back to the solution obtained in the arclength reference frame (the intrinsic coordinate system). Finally, we discuss non-monotone coordinate scalings and their application for finding self-intersections of vortex filaments. These self-intersecting vortex filaments are unstable and collapse into other structures or dissipate completely.

II. FORMULATION AND SCALING THE LIA

Alternate scaling of the LIA can be useful both for physical analysis and for computational reasons. For instance, the infinite domain due to $x \in \mathbb{R}$ can be mapped into a closed and bounded interval, which can assist with analytical and numerical analysis. We first determine the influence of such transforms. Let us consider the scaled

position vector

$$\mathbf{r} = f(x)\mathbf{i}_x + y(x,t)\mathbf{i}_y + z(x,t)\mathbf{i}_z\,, \tag{1}$$

where $f(x)$ denotes a general scaling of the x-coordinate. This is one of two possible equivalent such scalings, with the other being

$$\mathbf{r} = x\mathbf{i}_x + y(f^{-1}(x),t)\mathbf{i}_y + z(f^{-1}(x),t)\mathbf{i}_z \tag{2}$$

provided f^{-1}, the inverse map of f, exists. For this reason, we will often be interested in monotone scalings f so that the inversion f^{-1} is well-defined. We chose to work with (1) as opposed to (2) since it gives more computationally tractable results. From (1), we compute

$$\mathbf{t} = \frac{d\mathbf{r}}{ds} = \frac{d\mathbf{r}}{dx}\frac{dx}{ds} = (f', y_x, z_x)\frac{dx}{ds}$$

and $\mathbf{v} = (0, y_t, z_t)$, where

$$\frac{dx}{ds} = \frac{1}{\sqrt{f'^2 + y_x^2 + z_x^2}}\,.$$

We then have $\kappa\mathbf{n} = \frac{d\mathbf{t}}{ds} = \frac{d\mathbf{t}}{dx}\frac{dx}{ds}$, giving

$$\begin{aligned}\kappa\mathbf{n} = &\left[f''(y_x^2+z_x^2) - f'(y_xy_{xx}+z_xz_{xx})\right]\frac{dx}{ds}\mathbf{i}_x\\ &+\left[y_{xx}z_x - y_xz_xz_{xx} + y_{xx}f'^2 - f'f''y_x\right]\frac{dx}{ds}\mathbf{i}_y\\ &+\left[z_{xx}y_x^2 - z_xy_xy_{xx} + z_{xx}f'^2 - f'f''z_x\right]\frac{dx}{ds}\mathbf{i}_z\,,\end{aligned}$$

so that $\mathbf{v} = \gamma\kappa\mathbf{t}\times\mathbf{n} = \gamma\mathbf{t}\times(\kappa\mathbf{n})$ becomes

$$\begin{aligned}\mathbf{v} = &\gamma(y_xz_{xx} - z_xy_{xx})\left(\frac{dx}{ds}\right)^3\mathbf{i}_x\\ &-\gamma(f'z_{xx} - f''z_x)\left(\frac{dx}{ds}\right)^3\mathbf{i}_y\\ &+\gamma(f'y_{xx} - f''y_x)\left(\frac{dx}{ds}\right)^3\mathbf{i}_z\,.\end{aligned}$$

Matching the two representation of $\mathbf{v}$, we obtain the constraint $y_xz_{xx} - z_xy_{xx} = 0$ and the real-valued system

$$y_t = -\gamma(f'z_{xx} - f''z_x)\left(\frac{dx}{ds}\right)^3,$$

$$z_t = \gamma(f'y_{xx} - f''y_x)\left(\frac{dx}{ds}\right)^3.$$

Introducing the complex potential function

$$\Phi(x,t) = y(x,t) + iz(x,t)\,,$$

the PDE system reduces to

$$i\Phi_t + \gamma\left(f'\Phi_{xx} - f''\Phi_x\right)\left(f'^2 + |\Phi_x|^2\right)^{-3/2} = 0\,. \tag{3}$$

Note that (3) is a complicated nonlinear Schrödinger equation with variable coefficients (f' and f'' in general depend on x). However, with the scaling $\Phi(x,t) = \Psi(\mu,t)$ where $\mu = f(x)$, we may reduce (3) to

$$i\Psi_t + \gamma\left(1 + |\Psi_\mu|^2\right)^{-3/2}\Psi_{\mu\mu} = 0\,, \tag{4}$$

for non-degenerate f. Hence, (3) yields solutions of the LIA. The transformed equation (4) matches exactly that studied in [8, 9].

The form of (3) (and hence (4)) is $U(1)$-invariant, just like many of it's derivative NLS relatives, hence it makes sense to consider stationary solutions of the form $\Phi(x,t) = e^{-i\gamma t}\phi(x)$ to (3) (and $\Psi(\mu,t) = e^{-i\gamma t}\psi(\mu)$ to (4)).

To summarize, the permitted scalings are that for which:
(i) the LIA is invariant under monotone scalings of the x coordinate;
(ii) the LIA is invariant under scalings of the form $e^{-i\gamma t}$.

Together, these conditions guarantee the existence of planar vortex filaments described by $\Psi(x,t) = e^{-i\gamma t}\psi(\mu(x))$. In the extrinsic three-dimensional Cartesian frame, the position of the planar vortex filament at any time t is then given by

$$\mathbf{r} = \mu(x)\mathbf{i}_x + \cos(\gamma t)\psi(\mu(x))\mathbf{i}_y - \sin(\gamma t)\psi(\mu(x))\mathbf{i}_z\,, \tag{5}$$

To better visualize such vortex filaments, see Fig. 1, where we consider a periodic function $\psi(\mu(x))$. The vortex filament rotates about the x-axis as time increases. So, by determining $\psi(\mu(x))$, we determine the spatial structure of the planar vortex filament completely, the inclusion of a factor $e^{-i\gamma t}$ providing the motion of such a filament in time.

III. ACCURATE PERTURBATION APPROACH FOR THE STATIONARY SOLUTION

Let us consider the stationary solution $\Psi(\mu,t) = Ae^{-i\gamma t}\psi(\mu)$ to the scaled equation (4), where we let the parameter $A > 0$ hold the amplitude and normalize $\max\psi = 1$. Then, we obtain the ordinary differential equation

$$\psi + \left(1 + A^2\psi'^2\right)^{-3/2}\psi'' = 0\,. \tag{6}$$

The simplest nonlinear approximation to equation takes the form

$$\psi + \left(1 - \frac{3}{2}A^2\psi'^2\right)\psi'' = 0\,. \tag{7}$$

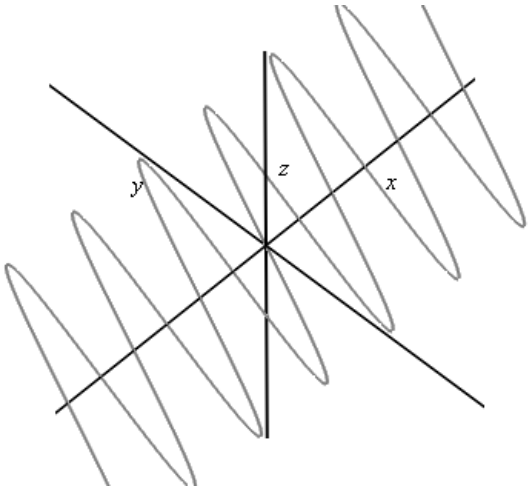

FIG. 1: Plot of the spatial geometry. The curve represents the planar vortex filament described by $\Phi(x,t) = e^{-i\gamma t}\phi(\mu(x))$ for periodic $\psi(\mu(x))$. As time increases, the structure rotates about the x-axis.

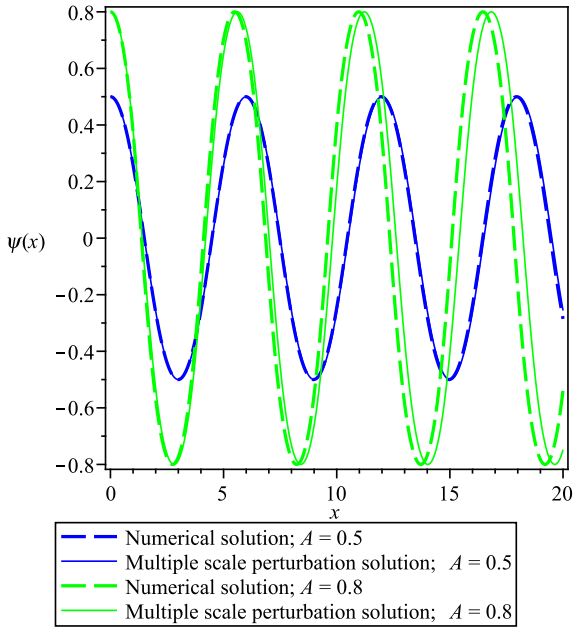

FIG. 2: (Color online) Plot of the perturbation solutions (13) for $\psi(x)$ obtained through the method of multiple scales against numerical solutions obtained via the Runge-Kutta-Fehlberg method (RKF45) [16]. The valid region for the approximation (7) is $A < 1/\sqrt{3} \approx 0.577$, and in this region the results agree nicely. For larger A, the agreement breaks down, as the solutions fall out of resonance with the true solutions.

As discussed in a forthcoming work, (7) has periodic real-valued solutions for $A < 1/\sqrt{3} \approx 0.577$. For small A, (7) is a good approximation to (6). It then makes sense to consider a perturbation solution, in terms of small parameter A^2. However, standard perturbation will yield inaccurate solutions which fall out of resonance with the true solution due to the appearance of secular terms. Hence, we shall be interested in applying the method of multiple scales to (7). To proceed, assume there exists parameter $\delta(A^2)$ such that $d/d\mu = \delta(A^2)(d/d\eta)$ where $\eta = \delta(A^2)\mu$. Then, we consider the perturbation solution $\psi(\mu) = \hat{\psi}(\eta; A^2) = \psi_0(\eta; A^2) + A^2\psi_1(\eta; A^2) + O(A^4)$, $\delta(A^2) = \delta_0 + A^2\delta_1 + O(A^4)$. Equation (7) becomes

$$\hat{\psi} + \delta^2\left(1 - \frac{3}{2}A^2\delta^2\hat{\psi}_\eta^2\right)\hat{\psi}_{\eta\eta} = 0\,, \tag{8}$$

giving

$$\delta_0^2\psi_{0,\eta\eta} + \psi_0 = 0\,, \quad \psi_0(0) = 1\,, \quad \psi_{0,\eta}(0) = 0\,, \tag{9}$$

$$\begin{aligned}\delta_0^2\psi_{1,\eta\eta} + \psi_1 &= \frac{3}{2}\delta_0^4\psi_{0,\eta}^2(\psi_0)_{\eta\eta} - 2\delta_0\delta_1\psi_{0,\eta\eta}\,,\\ \psi_1(0) &= 0 = (\psi_1)_\eta(0)\,.\end{aligned} \tag{10}$$

The quantities at $\eta = 0$ follow from the fact that we desire space-periodic ψ with amplitude A. As we assume a solution $\Psi = A\psi\exp(-i\gamma t)$, it follows that the amplitude of ψ must be 1 (then the amplitude of Ψ is A). Without loss of generality, we take $\eta = 0$ to correspond to a peak (this can be translated by $\eta -> \eta' + \eta_0$ if need be). Thus, $\psi_\eta(x) = 0$. Assuming $\psi = \psi_0 + A^2\psi_1 + \cdots$, it follows that $\psi_0(0) = 1$, $\psi_{0,\eta}(0) = 0$, $\psi_1(0) = 1$ and $\psi_{1,\eta}(0) = 0$.

Normalizing to get 2π-periodic solutions, we pick $\delta_0 = 1$, obtaining $\psi_0(\eta) = \cos(\eta)$. From here, we have

$$(\psi_1)_{\eta\eta} + \psi_1 = \left(2\delta_1 - \frac{3}{8}\right)\cos(\eta) + \frac{3}{8}\cos(3\eta)\,, \tag{11}$$

so picking $\delta_1 = 3/16$ prevents any secular terms. We then obtain

$$\psi_1(\eta) = \frac{3}{64}\left(\cos(\eta) - \cos(3\eta)\right) = \frac{3}{16}\sin^2(\eta)\cos(\eta)\,. \tag{12}$$

Therefore, we have obtained the perturbation solution

$$\begin{aligned}\psi(\mu) = &\cos\left(\left[1 + \frac{3}{16}A^2\right]\mu\right)\\ &+ \frac{3}{16}A^2\sin^2\left(\left[1 + \frac{3}{16}A^2\right]\mu\right)\cos\left(\left[1 + \frac{3}{16}A^2\right]\mu\right).\end{aligned} \tag{13}$$

Consider the standard case $\mu(x) = x$. From Eq. (13), we see that the approximate period of small-amplitude solutions satisfies

$$T(A) \approx 2\pi\left[1 + \frac{3}{16}A^2\right]^{-1} \approx 2\pi - \frac{3\pi}{8}A^2 + \frac{9\pi}{128}A^4\,. \tag{14}$$

In order to demonstrate the agreement between the solution (13) and the true solution, we plot the numerical solution along with the perturbation solution in Fig. 2. Since the perturbation and numerical results agree so nicely, the difference between the two is not easily ascertainable, so we plot their errors separately, in Fig. 3.

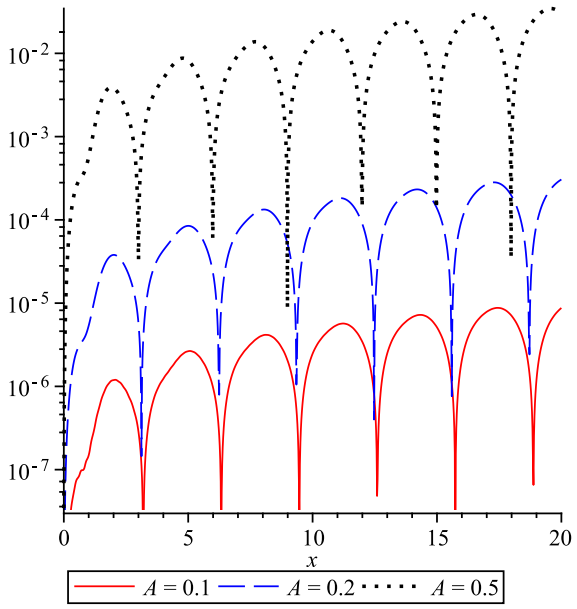

FIG. 3: (Color online) Plot of the absolute error between the perturbation solutions (13) for $\psi(x)$ obtained through the method of multiple scales and the numerical solutions obtained via the Runge-Kutta-Fehlberg method (RKF45) [16]. The agreement is strong for small amplitude solutions, while the agreement gradually breaks down for larger amplitudes.

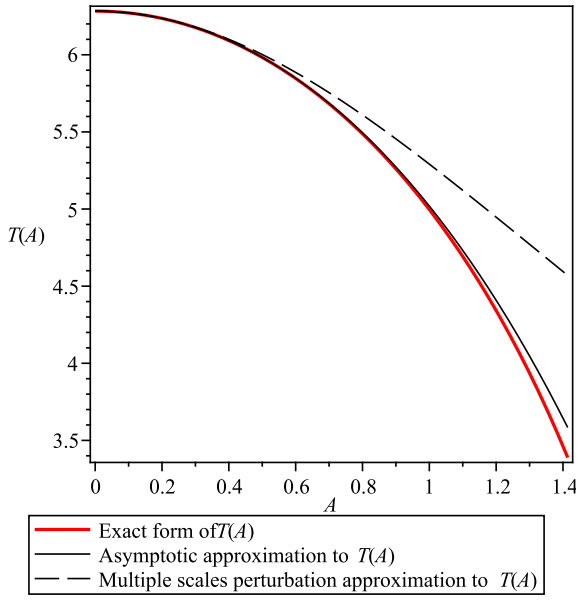

FIG. 4: (Color online) Plot of the x-period $T(A)$ for the stationary solution x-dependence function $\phi(x)$. In addition to the exact value (22), we plot two approximate quantities, namely the approximation found through multiple scales (14) and the asymptotic approximation (25) to the true result (22). We consider $A \in [0, \sqrt{2}]$.

IV. CONNECTION WITH ARCLENGTH SOLUTION AND IMPLICIT SOLUTION

In this section, take $\mu(x) = x$, so that $\Phi(x,t) = \Psi(\mu,t)$. In Van Gorder [13], an exact stationary solution for the arclength formulation of the LIA was given by

$$v(s,t) = e^{-it}q(s) = Be^{-it}\mathrm{sn}\left(\frac{s-\hat{s}}{\sqrt{1-B^2}}, Bi\right), \quad (15)$$

where B is the amplitude (in the arclength frame), $\hat{s}$ is a constant, and s is the arclength element. It was shown in [12] that the Cartesian quantity $\Phi(x,t)$ and the arclength quantity $v(s,t)$ are related by

$$|\Phi_x|^2 = \frac{2|v|^2}{(1-|v|^2)^2}, \quad \frac{dx}{ds} = \frac{1-|v|^2}{1+|v|^2}. \quad (16)$$

Noting that $|\Phi_x| = \phi'(x)$ and $|v| = q(s)$, we have that $\phi'^2 = 2q^2(1-q^2)^{-2}$. Separating variables, and using the form of dx/ds given in (16), we obtain

$$\phi(x) = \sqrt{2}\int_{\hat{s}}^{s(x)} \frac{B\mathrm{sn}\left(\frac{s-\hat{s}}{\sqrt{1-B^2}}, Bi\right)}{1+B^2\mathrm{sn}^2\left(\frac{s-\hat{s}}{\sqrt{1-B^2}}, Bi\right)} ds. \quad (17)$$

Performing the integration exactly is not possible (in closed form). And then, one must still contend with the arclength variable $s(x)$. So, while this formula offers a connection between the exact arclength solution to the planar vortex filament problem and that of the Cartesian problem, it is not very practical. We can compare this formula to the direct solution for $\phi(x)$. A first integral of (6) (when $\mu = x$ and hence $\psi(\mu) = \phi(x)$) is

$$\phi^2 - \frac{2}{A^2\sqrt{1+A^2\phi'^2}} = -\mathcal{E}. \quad (18)$$

If $\phi(0) = 1$, $\phi'(0) = 0$, then $\mathcal{E} = (2-A^2)/A^2 > 0$ since $|A| < \sqrt{2}$ for any periodic solution. Solving (18) for ϕ' and separating variables as needed,

$$x = \pm\int_{\phi}^{1} \frac{A^3(\zeta^2+\mathcal{E})}{\sqrt{4-A^4(\zeta^2+\mathcal{E})^2}} d\zeta. \quad (19)$$

Changing variables to $\xi = \zeta^2 + \mathcal{E}$,

$$x = \pm\frac{A^3}{2}\int_{\phi^2+\mathcal{E}}^{2/A^2} \frac{\xi d\xi}{\sqrt{(\xi-\mathcal{E})(2-A^2\xi)(2+A^2\xi)}}. \quad (20)$$

Eq. (20) is an implicit solution which is not easily inverted. However, we may still extract information out of this relation more easily than is the case when dealing with (17). In the previous section, we approximated the period of a space-periodic planar vortex filament using perturbation. We shall now be interested in comparing that approximation with a true exact relation between the period T and amplitude A for a space-periodic solution to the vortex filament problem.

If we consider the phase portrait, a quarter-period $T(A)/4$ occurs when ϕ goes from $\phi = 0$ to $\phi = 1$, so

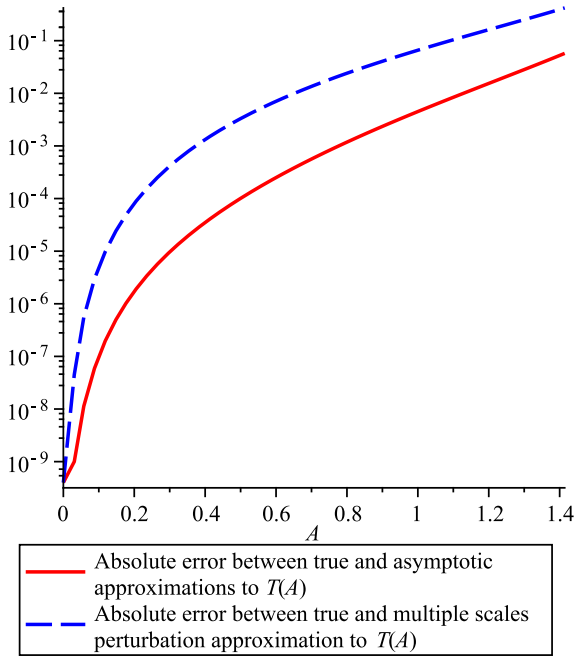

FIG. 5: (Color online) We demonstrate the relative error between the approximations to the period $T(A)$ and the true solution (22). Both are extremely accurate for small A, and gradually lose accuracy for larger A, though the asymptotic approximation (25) outperforms the multiple scale approximation (14) nicely. That said, in it's region of validity ($A < 1/\sqrt{3}$), the multiple scale approximation (14) is rather accurate for only a first order perturbation result.

from Eq. (20) we obtain the exact yet implicit relation

$$T(A) = 2A^3 \int_{\mathcal{E}}^{2/A^2} \frac{\xi d\xi}{\sqrt{(\xi - \mathcal{E})(2 - A^2\xi)(2 + A^2\xi)}} \,. \quad (21)$$

Now, in the valid region $0 < A < \sqrt{2}$, the definite integral (21) can be evaluated in terms of elliptic integrals to give the relation

$$T(A) = 8E\left(A/2\right) - 4K\left(A/2\right) \,, \quad (22)$$

where K is the complete elliptic integral of the first kind and E is the complete elliptic integral of the second kind. Recall that the period of the solutions in the arclength representation [13], the period of the space-periodic solution was a bit simpler, involving only the elliptic integral K.

In order to extract more information from Eq. (22), we turn to the small-θ asymptotics

$$K(\theta) = \frac{\pi}{2}\left(1 + \frac{1}{4}\frac{\theta^2}{1-\theta^2} - \frac{1}{8}\frac{\theta^4}{1-\theta^2}\right) \,, \quad (23)$$

$$E(\theta) = \frac{\pi}{2}\left(1 - \frac{1}{4}\theta^2 - \frac{3}{64}\theta^4\right) \,. \quad (24)$$

Using (23)-(24) in (22), and approximating where needed,

$$T(A) \approx 2\pi - \frac{3\pi}{8}A^2 - \frac{7\pi}{256}A^4 \,. \quad (25)$$

Note that the approximation (25) to the period $T(A)$ obtained through the fully nonlinear relation (20) for ϕ is in extremely good agreement with the approximation obtained through the method of multiple scales (14) for the period $T(A)$. In Fig. 4, we plot the exact period $T(A)$ found in (22), along with the approximations shown in (14) and (25). In Fig. 5, we plot the relative error between the approximations and the exact values.

V. NON-MONOTONE SPACE SCALES AND NUMERICAL SELF-INTERSECTION OF FILAMENTS

Up to this point we have considered only monotone scalings $f(x)$ in (1), since these permit well-behaved solutions to (4). As we've shown, such solutions can be studied analytically, and in some cases exactly. However, in situations where $f(x)$ is non-monotone, we may still assume a stationary solution of the form $\Phi(x,t) = e^{-i\gamma t}\phi(x)$. While $\psi(\mu)$ from (6) was defined on the real μ-axis in the case of monotone $\mu = f(x)$, for non-monotone $f(x)$ it is possible that the domain of $\phi(x)$ will be restricted. Assuming a solution $\Phi(x,t) = e^{-i\gamma t}\phi(x)$, (3) reduces to

$$\phi + \frac{f'\phi'' - f''\phi'}{\left(f'^2 + \phi'^2\right)^{3/2}} = 0 \,. \quad (26)$$

The ordinary differential equation (26) is degenerate when f is not strictly monotone, i.e. if there exists a point $x = a$ at which $f'(a) = 0$. In order for a planar vortex filament to have self-intersections, there should exist points $x_* < x^*$ such that $f(x_*) = f(x^*)$ and $\phi(x_*) = \phi(x^*)$, but for $x_* < x_1 < x_2 < x^*$, $f(x_1) = f(x_2)$ and $\phi(x_1) = \phi(x_2)$ can not hold simultaneously. If such x_1 and x_2 exist, then there can be a loop (if not, then we just have a constant valued function). Then from (1) we must have $\mathbf{r}(x_*,t) = \mathbf{r}(x^*,t)$ for all $t \geq 0$. If we have such points $x_* < x_1 < x_2 < x^*$, there there is at least one loop formed. This loop is parametrized by $\theta \in [x_*, x^*]$ as

$$r(\theta,t) = f(\theta)\mathbf{i}_x + \cos(\gamma t)\phi(\theta)\mathbf{i}_\mathbf{y} - \sin(\gamma t)\phi(\theta)\mathbf{i}_z \,, \quad (27)$$

with the loop closing since $\mathbf{r}(x_*,t) = \mathbf{r}(x^*,t)$. In Fig. 6 we provide a schematic of the planar loop vortex filament. Now that we have some conditions on parametrized crossings and loop strictures on a vortex filament, we provide some examples to show that these structures can actually occur as solutions to the equation governing a vortex filament of planar type.

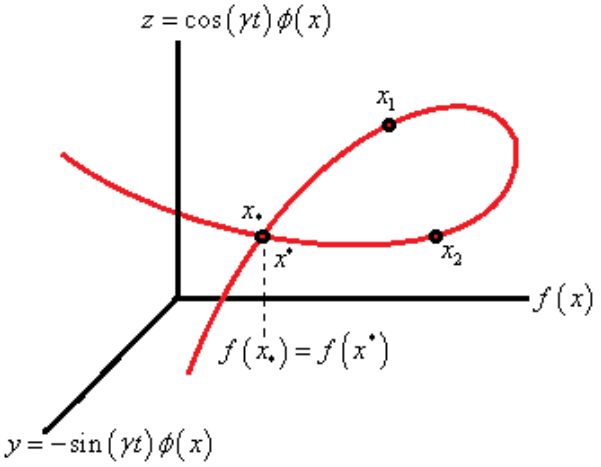

FIG. 6: Schematic of a self-intersection for the planar vortex filament governed by a solution $\phi(x)$ to equation (26). Self-intersection occurs at spatial coordinate $f(x_*)$ where the parametrization x attains the value x^* such that $f(x_*) = f(x^*)$ and $\phi(x_*) = \phi(x^*)$. It is necessary for $\phi(x_1) \neq \phi(x_2)$ for all $x_* < x_1 < x_2 < x^*$ in order to have a single loop. For multiple loops, similar yet more complicated conditions must hold.

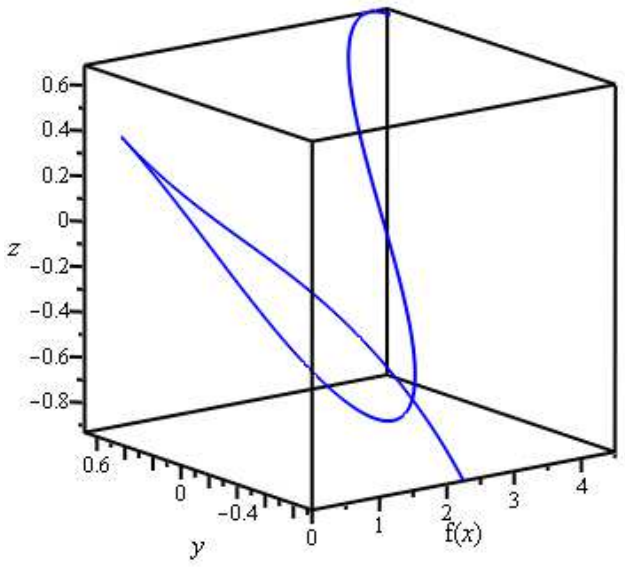

FIG. 7: Plot of the numerical solution for a single loop vortex filament described by $\phi(x)$ when $\phi(x)$ satisfies (28), $\phi(0.1) = 0.6$, $\phi'(0.1) = -0.1$. The x scaling is $f(x) = x^2/2$. The space coordinate is parametrized by $x \in [-2.12, 3.00]$.

A. Single loop case

As our first numerical case, we consider an example of a parametrized single loop on a vortex filament. Let us consider the scaling $f(x) = x^2/2$. We then have

$$\phi + \frac{x\phi'' - \phi'}{\left(x^2 + \phi'^2\right)^{3/2}} = 0\,. \tag{28}$$

Unlike in the simpler case of monotone f, here we cannot easily solve the differential equation (28) analytically. So, we resort to numerical solutions. It is useful to assign a specific x_N as a numerical initial point. Picking $x_N = 0$ is problematic, since (28) is degenerate at that point. So, we shall take x_N to be small yet positive. We find that loops are not obtained for many parameter values. However, they can occur for our choice of f. Taking, for instance, $x_N = 0.1$, $\phi(x_N) = 0.6$, $\phi'(x_N) = -0.1$, we find that $\phi(2.059) = \phi(-2.059)$ while $f(x) = f(-x)$ by the form of f selected, so we pick $x_* = -2.059$ and $x^* = 2.059$. To make sure the loop is closed, the derivatives should differ at each point. We calculate $\phi'(x_*) = 3.589$ while $\phi'(x^*) = 0.857$, so the loop does close. So, in the prescribed geometry, we have found a closed filament loop. As mentioned above, the loop must remain closed for all $t \geq 0$. The resulting single loop planar vortex filament is displayed in Fig. 7.

B. Double loop case

Let us now consider a double loop structure on a vortex filament. Let us take the scaling $f(x) = \cos(x)$. We then have

$$\phi + \frac{-\sin(x)\phi'' + \cos(x)\phi'}{\left(\sin^2(x) + \phi'^2\right)^{3/2}} = 0\,. \tag{29}$$

Taking $x_N = 0.1$, $\phi(x_N) = 0.5$, $\phi'(x_N) = -0.095$, we numerically solve (29). Defining $-x_*^{[1]} = 2.35 = x^{*[1]}$, $x_*^{[2]} = -3.89$, $x^{*[2]} = 2.395$, we have that $\phi(x_*^{[1]}) = \phi(x^{*[1]})$ and $\phi(x_*^{[2]}) = \phi(x^{*[2]})$. Yet, since $f(x) = \cos(x)$, we have $f(x_*^{[1]}) = f(x^{*[1]})$ and $f(x_*^{[2]}) = f(x^{*[2]})$. So, the conditions for crossing are satisfied at spatial coordinates $\cos(x_*^{[1]}) = -0.70$ and $\cos(x_*^{[2]}) = -0.73$. We verify that the derivatives differ at each point, so the loop structures close off at the required points. (If the derivatives do not differ, then the filament my become tangent to itself, and therefore not close to form a loop, at the required point.) Hence, we have obtained a double loop structure on a vortex filament. The resulting double loop planar vortex filament is displayed in Fig. 8.

One may continue with multi-loop structures, but these get progressively harder to construct, since one must guess an appropriate transform of space variable $f(x)$ and deduce values of the crossings. Further, since this is done numerically (such analytical constructions are very challenging), there is a bit of guess work involved in the initial conditions which permit solutions $\phi(x)$ which allow for the crossings.

While these loop structures have been shown to exist numerically for appropriate scales f and planar components ϕ, in practice one would not expect these structures to persist. A more physically relevant situation would be

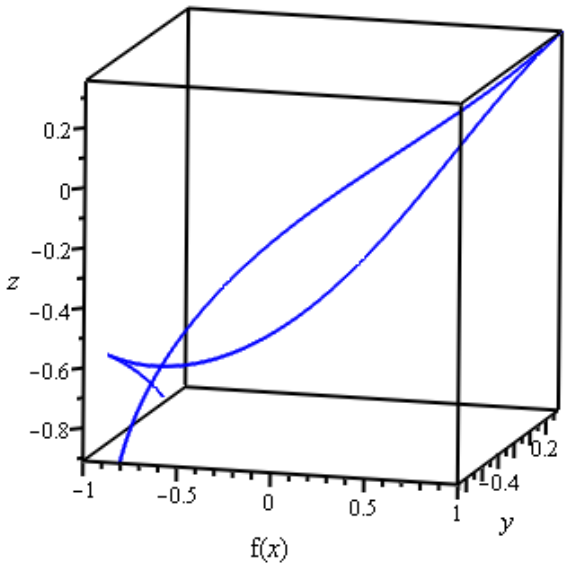

FIG. 8: Plot of the numerical solution for a double loop vortex filament described by $\phi(x)$ when $\phi(x)$ satisfies (29), $\phi(0.1) = 0.5$, $\phi'(0.1) = -0.095$. The x scaling is $f(x) = \cos(x)$. The space coordinate is parametrized by $x \in [-4.0, 2.5]$.

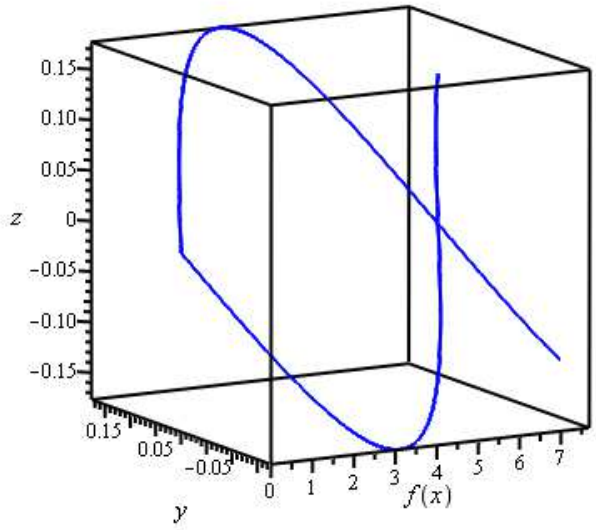

FIG. 9: Plot of the analytical solution for a single loop vortex filament described by $\phi(x)$ when $\phi(x)$ satisfies (32). The x scaling is $f(x) = x^2/2$, while the amplitude of the solution is taken to be $A = 0.25$. The space coordinate is parametrized by $x \in [x_*(A), x^*(A)]$ while on the loop.

for a vortex filament to cross (or come close to crossing, since physically the vortex core has non-trivial diameter), a loop structure is monentarily formed, and then the filament is disrupted. Depending on the ambient fluid, one could have that (i) the vortex filament sheds the loop, and realign as a non-crossing well-defined curve; (ii) the loop collapses, with the filament stretching laterally to realign as a non-intersecting curve; (iii) the loop dominates, with the "tails" decaying, resulting in a vortex ring. While the present results point toward either of those outcomes, note that one would need to retain more structure than the LIA permits in order to fully model the dynamics of such vortex filament crossings. In order to study such complicated dynamics, the full integral form of the BiotSavart law would be required. At best, the LIA provides a sort of first order approximation to such behavior, though it fails to pick up on the complicated dynamics of these situations, which would lead from a vortex filament crossing to one of the possible outcomes listed. That the LIA can pick up on the occurrence of such interactions, given it's simplicity relative to the full Biot-Savart law, is still beneficial.

C. Analytical calculation

While numerical results are easiest for the case of self-intersections, we remark that analytical approximations can be obtained, at a cost. Indeed, when $f'(x_0) = 0$ for some x_0, then (26) degenerates (the coefficient of ϕ'' vanishes, decreasing the order of the equation). To counter this, we must have two solution branches, which we match at x_0. However, while the matching preserves continuity, it cannot preserve continuity of the first derivative (on each side of x_0, that is $x < x_0$ and $x > x_0$, the slope of the branches must differ). Without loss of generality, take $x_0 = 0$. Then, in order to match a positive and negative branch, we consider the following piecewise defined solution:

$$\phi(x) = \begin{cases} -\psi(f(x)) & x_* < x < 0\,, \\ 0 & x = 0\,, \\ \psi(f(x)) & 0 < x < x^*\,, \end{cases} \tag{30}$$

where $\psi(\mu)$ is a solution as was found in the monotone case and $x_* < 0 < x^*$ such that $f(x_*) = f(x^*) = T/2$ where T is the period of ψ. From the form of (26), if ψ is a solution, then so is $-\psi$. Hence, each branch is a solution (when $f' \neq 0$). This representation is not unique, as we could have reversed the signs in (30). To get both functions to match at $x = 0$, we use a modified form of (13) where $\psi(0) = 0$, $\psi'(0) = 1$ (which gives a sine, as opposed to cosine, representation). This is equivalent to translation of the solution in (13) by $-\pi/2$ on the x-axis. So, to lowest order (one can add higher order corrections, but we suppress them for brevity) (30) becomes

$$\phi(x) = \begin{cases} -\sin\left(\left[1 + \frac{3}{16}A^2\right] f(x)\right) & x_* < x < 0\,, \\ 0 & x = 0\,, \\ \sin\left(\left[1 + \frac{3}{16}A^2\right] f(x)\right) & 0 < x < x^*\,. \end{cases} \tag{31}$$

Note that $\phi(x_*) = -\psi(f(x_*)) = -\psi(T/2) = 0 = \psi(T/2) = \psi(f(x^*)) = \phi(x^*)$ by construction, so $\phi(x_*) = \phi(x^*)$.

For example, consider again the $f(x) = x^2/2$ case. We pick

$$x_*(A) = -\sqrt{2\pi\left[1+\frac{3}{16}A^2\right]^{-1}},$$

$$x^*(A) = \sqrt{2\pi\left[1+\frac{3}{16}A^2\right]^{-1}}.$$

We then get (to lowest order)

$$\phi(x) = \begin{cases} -\sin\left(\left[1+\frac{3}{16}A^2\right]\frac{x^2}{2}\right) & x_*(A) < x < 0\,, \\ 0 & x = 0\,, \\ \sin\left(\left[1+\frac{3}{16}A^2\right]\frac{x^2}{2}\right) & 0 < x < x^*(A)\,. \end{cases} \tag{32}$$

Note that $\phi(x_*(A)) = -\sin(\pi) = 0 = \sin(\pi) = \phi(x^*(A))$. Furthermore, let

$$x_1(A) = -\sqrt{\pi\left[1+\frac{3}{16}A^2\right]^{-1}},$$

$$x_2(A) = \sqrt{\pi\left[1+\frac{3}{16}A^2\right]^{-1}}.$$

Then $\phi(x_1(A)) = -\sin(\pi/2) = -1 \neq 1 = \sin(\pi/2) = \phi(x_2(A))$. So, there exist $x_1(A)$ and $x_2(A)$ such that $x_*(A) < x_1(A) < x_2(A) < x^*(A)$, $\phi(x_*(A)) = \phi(x^*(A))$, and $\phi(x_1(A)) \neq \phi(x_2(A))$, so a loop is indeed formed. The solution (32) is shown in Fig. 9, in the case of $A = 0.25$. The single-loop structure is prominent.

We remark that since ϕ is continuous on $x \in [-\sqrt{\pi}, \sqrt{\pi}]$, yet ϕ' has a discontinuity at a single point $x = 0$, the matched solution is a class of "weak" solution.

VI. CONCLUSIONS

We have derived the fully nonlinear form of the local induction approximation (LIA) governing the motion of a vortex filament. Permitting a scaling of the free coordinate along which the vortex is aligned (x, in our case) permits us to have greater flexibility in computing solutions, both analytically and numerically. Such vortex solutions are a variation on the theme of planar vortex filaments, and take the form

$$\mathbf{r} = (f(x), \cos(\gamma t)\phi(x), -\sin(\gamma t)\phi(x))\,.$$

The main analytical benefit is that such a solution form can capture a greater range of physical behaviors (particularly when the scale is non-monotone), while numerical simulations can be made easier by taking a scale $f : \mathbb{R} \to \mathcal{I}$ where $\mathcal{I}$ is a compact interval (numerical integration on such a compact interval can often be simpler than on an unbounded domain such as the real line).

In the case of monotone scalings $f(x) = \mu$, we have a very elegant way to determine the planar contribution $\phi(x) = \psi(\mu)$ to the vortex filament structure, obtaining a nonlinear ordinary differential equation (ODE) governing ψ; see (6). For monotone scalings, we therefore find that ψ is a strict function of μ and therefore the ODE (6) has only constant coefficients, making it's solution possible. The planar solution is equivalent to a stationary solution of the form $\Phi = e^{-\gamma t}\psi(\mu)$. The main stationary solution of interest is periodic for small amplitudes A, so this is the solution we focus on in Section 3. While numerical solutions can be obtained, we compute a perturbation solution, scaling both the function and the variable by the amplitude A of solutions through a multiple scales approach. We compare the perturbation solution to numerical solutions, finding that the perturbation solution accurately captures the structure of the planar vortex filament (in particular, the spacial period of oscillation for such solutions). We find that the spatial period $T(A)$ is given by the approximation

$$T(A) \approx 2\pi\left(1+\frac{3}{16}A^2\right)^{-1},$$

for small A.

Properties of the planar vortex filament in the arclength system (the intrinsic coordinate frame) were considered in [13], and in Section 4 we have compared the two formulations. The primary benefit of the arclength frame is that it allows for exact solutions, in terms of elliptic sn functions. The Cartesian framework, however, gives us a clearer view of exactly what is going on with the structure of the vortex filament. While there is no exact solution, the perturbation result does work nicely for small amplitude periodic solutions. Despite the fact that there is no exact closed-form solution for $\psi(\mu)$, we are able to derive an exact relation for the period $T(A)$ in terms of elliptic integrals, obtaining

$$T(A) = 8E\left(A/2\right) - 4K\left(A/2\right),$$

which agrees nicely with the approximation found through perturbation for small A; see Fig. 4. This is also reminiscent of the period for the arclength representation of the planar solution discussed in [13]. Note that there is a bound $A < \sqrt{2}$ on the amplitude A of the space-periodic function $\psi(\mu)$, as will be discussed in a forthcoming work. As such, the maximal period occurs with amplitude $A = 0$ and is $T(0) = 2\pi$ while the minimal period solution occurs with amplitude $A = \sqrt{2}$ and is $T(\sqrt{2}) = 3.3886$. Hence, the period $T(A)$ of a space-periodic solution is related in an inverse manner to the amplitude A of such a solution.

For monotone scalings f we were able to obtain the nice analytical results discussed above. We also discuss non-monotone coordinate scalings f and their applica-

tion for finding self-intersections of vortex filaments. An equation governing the stationary solution $\phi(x)$ was given in (26). This equation becomes singular at points where monotonicity of f fails, yielding solutions which, in some cases, permit self-intersection of the curve $\mathbf{r}$ given in (1). Such a self-intersection results in a vortex filament loop. While such a situation is not tractable analytically, we provide numerical simulations to demonstrate that such results are at the very least mathematically possible. We also outline some general criteria which would permit a loop filament structure. These self-intersecting vortex filaments essentially "break" the LIA formulation, meaning that once intersection occurs, the LIA is not sufficient to study the dynamics of the loop solutions. Such solutions are likely unstable and collapse into other structures or dissipate completely. These types of dynamics are quite interesting, and would certainly merit future work. Analytical results, under weaker conditions than monotonicity, yet stronger conditions than just arbitrary non-monotone transforms, could be possible, maybe in the case of the specific examples considered here. Some analytical results were given for the non-monotone scalings, and it was shown that such solutions may be constructed in a piecewise manner. These analytical solutions are continuous, yet fail to have a continuous derivative. In this sense, we may view such solutions as weak solutions. Nevertheless, these analytical results agree qualitatively with the numerical simulations.

Acknowledgements

R.A.V. supported in part by NSF grant # 1144246. The author appreciates the comments of the reviewers, which have led to improvement in the paper.

[1] L.S. Da Rios, Rend. Circ. Mat. Palermo 22, 117 (1906).
[2] R.J. Arms and F.R. Hama, Phys. Fluids 8, 553 (1965).
[3] R.L. Ricca, Nature 352, 561 (1991).
[4] S. Kida, J. Fluid Mech. 112, 397 (1981).
[5] R.L. Ricca, Chaos 3, 83 (1993); R.L. Ricca, D.C. Samuels, and C.F. Barenghi, J. Fluid Mech. 391, 29 (1999); F. Maggioni, S.Z. Alamri, C.F. Barenghi, and R.L. Ricca, Nuovo Cimento C 32, 133 (2009); F. Maggioni, S.Z. Alamri, C.F. Barenghi, and R.L. Ricca, Phys. Rev. E 82, 026309 (2010).
[6] T. Lipniacki, J. Fluid Mech. 477, 321 (2003).
[7] R.L. Ricca, Physics of Fluids A 4, 938 (1992).
[8] R.A. Van Gorder, Theor. Comput. Fluid Dyn. 26, 161 (2012).
[9] R.A. Van Gorder, Theor. Comput. Fluid Dyn. 26, 591 (2012).
[10] V.P. Dmitriyev, Am. J. Phys. 73, 563 (2005).
[11] B.K. Shivamoggi and G.J.F. van Heijst, Physics Letters A 374, 1742 (2010).
[12] M. Umeki, Theor. Comput. Fluid Dyn. 24, 383 (2010).
[13] R. A. Van Gorder, Phys. Rev. E 86, 057301 (2012).
[14] H. Hasimoto, J. Fluid Mech. 51, 477 (1972).
[15] H. Hasimoto, J. Phys. Soc. Japan 31, 293 (1971).
[16] E. Fehlberg, Computing (Arch. Elektron. Rechnen) 6, 61 (1970).